Facies (2009) 55:37–46
DOI 10.1007/s10347-008-0160-6

ORIGINAL ARTICLE

Extrapolation of depositional geometries of the Menorcan Miocene carbonate ramp with ground-penetrating radar

U. Asprion · H. Westphal · M. Nieman · L. Pomar

Received: 28 September 2007 / Accepted: 22 August 2008 / Published online: 12 September 2008

Abstract The Tortonian carbonate ramp of Menorca was previously studied on the basis of outcrops along sea-cliff outcrops. These sea cliffs, in combination with inland water wells, are the basis for a facies model for the reconstruction of the internal architecture and for characterizing the internal heterogeneities of this carbonate platform. However, any such three-dimensional reconstruction is generally limited by the given geometrical arrangement of the two-dimensional outcrops and the uncertainties of correlation with the one-dimensional wells. Here, ground-penetrating radar (GPR) has been employed in order to test and refine the depositional model. Although GPR is well known for being an excellent tool for high-resolution underground studies of sedimentary systems, the application for studying carbonate rocks is still far from routine. The reason for this discrepancy is two-fold: the minor mineralogical contrast between lithologies in carbonate rocks results in subtle reflections, and, even more important, the porosity structure in carbonates is thoroughly and repeatedly changed during diagenesis, commonly across the different facies, leading to problems in predictability of the petrophysical properties. The study of the Menorcan carbonate ramp with large distance–deep penetration GPR sections demonstrates that in spite of these difficulties, GPR is a valuable tool for extrapolating information from outcrops and wells. It is useful for characterizing heterogeneities larger than outcrop scale.

Keywords Ground-penetrating radar · Lower Tortonian · Carbonate platform · Menorca · Depositional geometries · Progradation

U. Asprion (✉)
Institut für Geologie, Callinstr. 30,
30167 Hannover, Germany
e-mail: u.asprion@gmx.de

H. Westphal
Fachbereich Geowissenschaften, Universität Bremen,
Leobener Straße, 28359 Bremen, Germany

M. Nieman
Geoservices, B.P. 20, 7, rue Isaac Newton,
93 151 Le Blanc-Mesnil, France

L. Pomar
Departament de Ciències de la Terra,
Universitat de les Illes Balears, 07071 Palma, Spain

Introduction

On the island of Menorca (Balearic Islands, Spain), a Lower Tortonian carbonate ramp is well exposed on sea cliffs. On the basis of such sea-cliff outcrops complemented by inland water wells, the platform architecture has been shown to represent a distally steepened ramp with a strong dominance of rhodoliths and heterotrophic organisms (Obrador 1972–1973; Obrador et al. 1983, 1992; Pomar et al. 2002, 2004). These outcrop studies have revealed that this ramp is characterized by pronounced shore-parallel transport of carbonate sediment along the ramp and ramp slope, and by channelized transport of sediment from the ramp top and slope to the toe of slope.

Even though the outcrops provide detailed information on the geometries, the lateral extension of the outcrops limits the characterization of heterogeneities larger than outcrop scale. The wells provide one-dimensional information only that necessarily leaves some uncertainty in terms of correlation. The approach of the present study is to extrapolate the information gathered from outcrops and wells into the shallow subsurface by using ground-penetrating radar

(GPR) profiles, improving and extending the three-dimensional information on the architectural heterogeneities of this carbonate ramp.

The approach presented here goes beyond the academic interest in understanding the genetic factors that controlled the depositional system. Three-dimensional information on the distribution of sedimentary facies is mandatory for reservoir-quality characterization, aquifer properties identification, and environmental geology. Especially for improved modeling of fluid movement in aquifers and for hydrocarbon resource management, high-resolution 3-D data are needed to capture medium- to small-scale heterogeneities related to sedimentary structures (Grasmueck and Weger 2002). In carbonate rocks, the field of high-resolution stratigraphic architecture is of increasing interest because of the outstanding importance of carbonate rocks as hydrocarbon reservoirs and aquifers. The complex facies architecture and complicated diagenetic history of carbonate rocks usually result in highly heterogeneous reservoir properties (Stoudt and Harris 1994). However, most seismic information is limited, at the best, to a resolution of 10 m, whereas the internal heterogeneities and many sedimentary structures that significantly influence fluid flow are on a smaller scale. Additionally, seismic techniques cannot be used in the shallow subsurface.

Outcrop analog studies have become an increasingly important tool to assess small-scale heterogeneities below the limit of seismic resolution (Mazzullo 1998; Borgomano et al. 2002). Nonetheless, it is a general problem of geological fieldwork that the limited extent of outcrops in most cases restricts the examination of lateral relationships and of three-dimensional geometries. Information from boreholes can complement outcrop information. However, as boreholes are one-dimensional, they can only provide limited information on lateral continuity.

Ground-penetrating radar offers a link between stratigraphic architecture data from outcrop to the shallow subsurface for reservoir-scale studies. It thus allows expanding information from outcrops to extensive high-resolution GPR sections that can be arranged as quasi-3D datasets. GPR represents an inexpensive and fast reconnaissance technique with high resolution of the shallow subsurface. GPR has been established as a standard too for the examination of siliciclastic sediments and rocks (e.g., Huggenberger et al. 1994; Stephens 1994; Bristow 1995; Asprion and Aigner 1997; McMechan et al. 1997; Corbeanu et al. 2001; Buynevich and Fitzgerald 2003). In contrast, the application to carbonate rocks still is far from routine. This difference between siliciclastic and carbonate deposits with respect to GPR studies stems from the fact that carbonates have minor mineralogical contrast between different lithofacies and, probably more important, that diagenesis of carbonate rocks results in a profound and repeated reorganization of pore geometries and pore volumes, fundamentally changing petrophysical properties (Anselmetti and Eberli 1993; Kenter et al. 1997). The acquisition and interpretation of GPR data from carbonate rocks therefore is by far less straightforward than for siliciclastic rocks. The few published GPR studies of carbonates deal, e.g., with a Silurian grainstone shoal (Pratt and Miall 1993), fractures within Mississippian carbonates (Liner and Liner 1995), the architecture of a shallow Jurassic limestone (Dagallier et al. 2000), Jurassic buildups (Asprion and Aigner 2000), Pleistocene oolite bodies (Grasmueck and Weger 2002), karst aquifers (Cunningham 2004), and Danian carbonate mounds (Nielsen et al. 2004). The present study presents the approach of using GPR sections for extrapolating facies information and geometries from outcrops and wells in order to refine and extend the resolution of the medium- and small-scale complexities in facies architecture.

Study area

This GPR study focuses on the Lower Tortonian carbonate ramp of Menorca previously described by Obrador (1972–1973), Pomar et al. (1983, 2002, 2004), Barón and Pomar (1985), Pomar (2001), Pomar et al. (2002), and Brandano et al. (2005). The island of Menorca, situated in the western Mediterranean, is the north-easternmost of the Balearic Islands. Upper Miocene (Lower Tortonian to Lower Messinian) carbonate sediments compose the southern part of the island (Fig. 1) and unconformably onlap tectonically

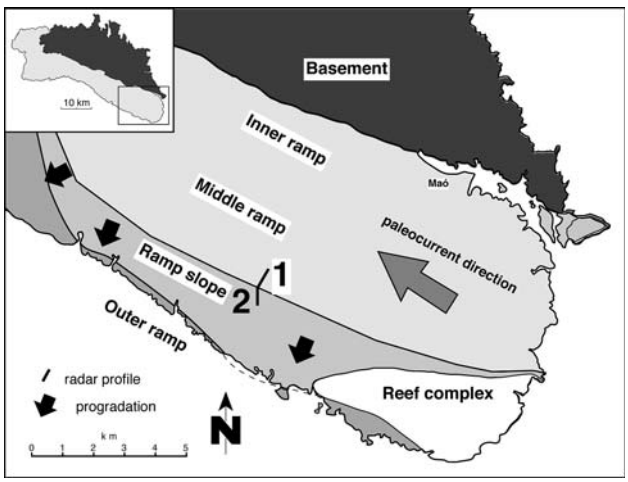

Fig. 1 Location of study area on Menorca. Facies distribution of the Lower Tortonian Lower Bar Unit and the overlying Reef Complex on the eastern side of SE-Menorca and location of the radar sections No. 1 and 2 on the middle to outer ramp of the Lower Bar Unit. *Inset* shows overview of the island and position of enlarged map

deformed Palaeozoic to Middle Miocene rocks (Obrador 1972–1973).

Upper Miocene rocks crop out on all Balearic Islands and have been subdivided into three sedimentary units (Pomar et al. 1983, 1996; Barón and Pomar 1985) interpreted as third-order depositional sequences sensu Haq et al. (1988) (Pomar et al. 1996): (1) The Lower Tortonian "Lower Bar Unit" on Menorca (Obrador et al. 1983, 1992; Pomar 2001; Pomar et al. 2002), corresponds to the "*Heterostegina* Calcisiltites" sensu Pomar et al. (1996) of Mallorca and is the focus of the study presented here. (2) The Upper Tortonian–Lower Messinian unit is termed "Reef Complex" (Obrador et al. 1983) and consists of a progradational coral-reef platform (Pomar 1991, 2001; Pomar et al. 1996). On Menorca outcrops of the "Reef Complex" are limited to a small area south of Maó (Fig. 1), south of Ciutadella and in the vicinity of Son Bou (Obrador et al. 1983). (3) Younger Messinian carbonate sediments, which include stromatolites, oolites, and marls crop out on other Balearic Islands but are absent on Menorca.

On the basis of extensive sea cliff outcrops and numerous water wells on Menorca, these deposits were interpreted to conform a distally steepened ramp sensu Read (1985) (Pomar 2001). Only minor post-depositional tectonic tilt has affected the ramp deposits (1–2° in depositional dip direction). As the ramp deposits are preserved close to the depositional orientation of the carbonate ramp they are ideally suited for studying the depositional geometries.

The transgressive systems tract of this third-order sequence is composed predominantly of nearshore large-scale cross-bedded pebbly siliciclastic sandstone units. The carbonate sediments that are the focus of this paper make up the highstand systems tract of this third-order sequence. They consist of aggrading and prograding carbonate sediments deposits. Four facies belts, broadly parallel to basement contours, are distinguished in dip direction: (1) inner ramp, (2) middle ramp, (3) ramp slope, and (4) outer ramp including the toe-of-slope deposits (Fig. 2; Pomar 2001; Pomar et al. 2002). The following description follows Pomar et al. (2002) and Mateu-Vicens et al. (2008) to where the reader is referred for more details. The GPR sections presented in this contribution record middle ramp to ramp slope facies.

Inner ramp

The inner ramp environment extended seawards from the palaeo-shoreline. Close to the shore, inner ramp deposits contain fan-delta sediments reworked in a shoreface environment. Facies consist of alluvial-fan conglomerates and sandstones, conglomeratic beachface deposits and structureless conglomerates and pebbly sandstones. The fan-delta deposits pass downdip into unsorted and burrowed mollusc-foraminifer packstones that are interpreted as shallow-water sediments baffled, trapped and sheltered in seagrass meadows.

Middle ramp

Basinward, inner ramp deposits interfinger with planar to cross-bedded grainstones. Common skeletal components are rhodoliths and fragments of red algae, echinoids, bryozoans and molluscs. Larger foraminifers (*Amphistegina* and some *Heterostegina* fragments) are common. These grainstones are interpreted as formed by medium 2D subaqueous dunes where the compound cross bedding was produced by the migration of superposed small bedforms (sensu Ashley 1990).

As inferred from bedding patterns and architectural reconstruction, the inner- and middle ramp together were deposited onto a gently seaward dipping surface extending basinward from the shoreline to the oligophotic zone, a depth at which carbonate production was dominated by red algae, larger benthic foraminifers and other benthic heterotrophs.

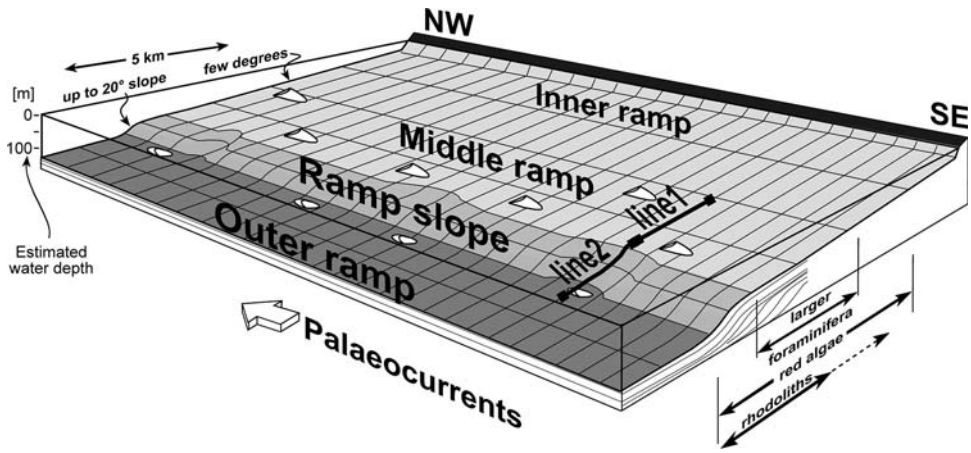

Fig. 2 Ramp depositional model (modified from Pomar 2001). Note occurrence of dunes in middle to outer ramp settings (Pomar et al. 2002)

Ramp slope

Upper ramp slope

Middle ramp deposits pass basinward into large-scale clinobeds that dip seaward at 15–20°. These clinobeds are composed of rhodolitic rudstones to floatstones and interlayered red-algal grainstones. The steepening in this part of the ramp is the result of increased sedimentation rate caused by combined accumulation of in situ production of gravel-sized skeletal components (rhodoliths) in the oligophotic zone, and of sand-sized sediment swept to the upper ramp slope from the shallower mesophotic zone. Bottom currents are thought to have kept the rhodoliths in motion and have removed fine-grained sediment (Pomar 2001; Pomar et al. 2002; Brandano et al. 2005). Water depths of the rhodolite-dominated carbonate production in the oligophotic zone are estimated to ranging between 40 and 80 m (Mateu-Vicens et al. 2008). The clinobeds laterally exceed the extension of individual outcrops of 100–200 m and prograded over a total distance of about 3 km.

Lower ramp slope

Seaward of the steep clinoforms, the inclination of the depositional profile progressively decreases again. Accumulation in this depositional setting was dominated by sediment gravity flows (turbiditic currents and debris-flows) and by settling of pelagic and hemipelagic sediments. The debris flow deposits are represented by structureless rudstones to floatstones, and locally grainstones and packstones, and the turbiditic deposits are represented by graded grainstones to packstones. Graded grainstones to wackestones occur in laterally extensive beds, where incised channels may be infilled by rhodolitic rudstone/floatstone and crossbedded grainstones. Locally, massive structureless packstones resulted from intense bioturbation of graded turbiditic deposits. Large volumes of the sediment transported downslope by gravity flows were reworked by bottom currents parallel to depositional strike, resulting in the formation of cross-bedded grainstone units. These grainstone units consist of 10 to 20 cm thick beds that stack in bed-sets up to a few meters in thickness. Cross bedding in these subaqueous dunes indicate western-directed transport and correspond to small-scale bedforms migrating parallel to the slope. The absence of in situ photic-dependent biota indicates deposition below the photic zone.

Outer ramp to toe-of-slope

The toe-of-slope is estimated to represent water depths of 80–100 m (Mateu-Vicens et al. 2008). The deeper part of the ramp is characterized by laminated fine-grained wackestones and packstones to grainstones. These deposits are horizontally bedded or dip gently (less than 10°) in basinward direction. They show slightly undulate bedding in strike direction with some 100 m in wavelength and up to 1–2 m in amplitude. Some of these wavy features are attributed to depositional processes but others are associated to shear bands related to synsedimentary gliding deformation. Locally, channel-like deposits, elongated in depositional dip direction, are encased in the wackestones and packstones. Interbedded graded beds are interpreted as distal turbidites.

In distal positions, the bedding dip angle decreases and the fine-grained wackestones and packstones are interbedded with large-scale cross-bedded grainstone units that are prism-shaped in section parallel to depositional strike, and mound-shaped in dip section. These grainstone units correspond to large 3D subaqueous dunes (sensu Ashley 1990) created by bottom currents flowing towards the NW, paralleling the depositional strike. The current-winnowed sands are platform/slope-derived and are embedded in the distal slope/outer ramp facies.

Methods

Ground-penetrating radar records the reflections of high-frequency electro-magnetic waves that are emitted into the ground, and partly reflected by structural heterogeneities that introduce changes in electrical properties. Such structural heterogeneities include changes in porosity and permeability, thus influencing water content that determines the amplitude of the reflections (Davis and Annan 1989; van Dam and Schlager 2000). Other heterogeneities can be related to the mineralogy and/or pore space fillings (van Dam and Schlager 2000). However, in pure carbonate systems this effect usually is minor. For a detailed discussion of the GPR method for geoscientific applications, the reader is referred to Conyers and Goodman (1997), Reynolds (1997), and Neal (2004).

For the present study, a transmitting-receiving antenna unit with a center-frequency of 300 MHz and a GSSI (Geophysical Survey Systems Inc.) High-power transmitter was moved along the profile lines. Measurements were taken every 0.1 m. The information was recorded as two-way-travel time (TWT). The data-acquisition procedure followed the protocols described by Davis and Annan (1989), Grasmück (1992) and Asprion (1998). The profile lines were chosen to follow public roads that allow for long straight profiles on even ground (Fig. 3a). Additionally, the asphalt cover keeps the ground humidity as constant as possible which is desirable for GPR. However, the number of artefacts is significantly higher along roads compared to the open fields. Such artefacts include surficial objects such

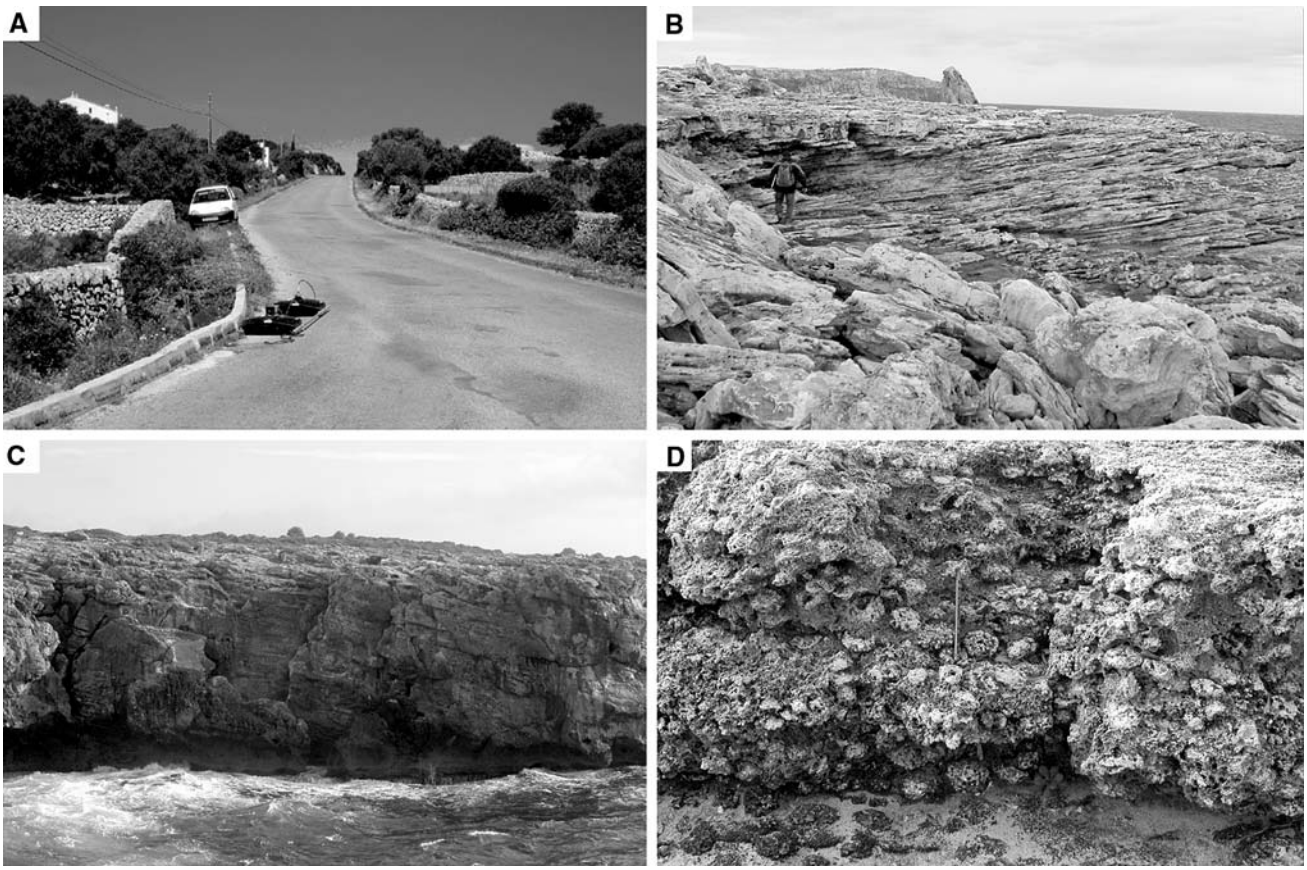

Fig. 3 **a** Outcrop photo showing the measuring conditions. View to the north from the end of GPR line 2. **b** Outcrop photograph showing the internal structure of longshore dunes. **c** Prograding clinoforms on the ramp slope; exposed on a modern sea cliff. **d** Outcrop photograph of coarse-grained rhodolitic clinobeds

as phone and power poles, and subsurface objects including cables, pipes and buried trenches. In addition, natural objects such as bushes and trees can introduce disturbances of the GPR records. The surficial objects were recorded on the section log for later identification on the GPR sections.

For depth conversion an average wave velocity of 0.12 m/ns was used that was derived from diffraction hyperbola analyses (this value corresponds to values given by Milsom 1996; Dagallier et al. 2000; Grandjean et al. 2000). We abstained from applying a common mid point correction, because of the inclination of the layers, rendering such a correction inaccurate (cf. Grandjean et al. 2000). The resolution of GPR is 0.5 of the radar wavelength (λ). The value of λ is the quotient of wave velocity (v) and frequency. The wave velocity v is defined as the quotient of the speed of light c and the square root of the relative dielectric permittivity ε_r $\left(v = \frac{c}{\sqrt{\varepsilon_r}}\right)$, where ε_r depends on the material passed by the signal and ranges from 1 for air to 81 for water. It follows from this equation that decreasing wavelengths result in increasing resolution where it penetrates a medium denser than air.

For the study presented here, the data were bandpass-filtered to remove noise. On some lines frequency-wave number filtering (fk filtering) was used to remove horizontal noise. In contrast to earlier high-resolution studies (e.g., Grasmueck and Weger 2002) we here apply GPR for covering sections of several 100 m length with a penetration of up to 30 m. The GPR data are then interpreted on the basis of a preexisting depositional model based on outcrops and well data.

Results and interpretation

Ground-penetrating radar usually reaches 100–200 ns TWT, roughly corresponding to depths of around 5–10 m for a typical average wave velocity of 0.1 m/s. In this study we were able to reach a maximum TWT of 500 ns, which corresponds to roughly 30 m penetration depth with a wave velocity of 0.12 m/ns derived from diffraction hyperbola analysis. This shows that the GPR signals in our study are faster than for average materials. According to the spectral analysis of the lines, the resolution of the 300-MHz antenna is around 0.3 m.

Middle ramp (position: Fig. 1, line 1; GPR section: Fig. 4a)

Data

This line covers a 597 m section of middle ramp to slope sediments. Between 20 and 150 m, 330–360 m, and 440–490 m of the section, penetration is very low. Therefore no interpretable data could be collected for these intervals. Between approximately 180 and 330 m, and between 490 and 597 m, penetration reaches an interpretable depth of approx 160 ns (approx. 10 m). In this part, high-amplitude reflections occur that show a dip of 12–19° in basinward (southern) direction. The individual reflections display disturbed geometries and cannot be followed downdip.

Interpretation

This section shows a general reflection dip of 12–19° to the south. The homogeneous radar facies is thought to correspond to the wackestone sediments with their relatively low porosity seen in outcrop. At 270 and at 560 m of the section onlapping reflection patterns are observed that are interpreted as results of sea-level variations (Fig. 4b, c, respectively). The quality of the data, i.e., the penetration, amplitude and continuity, varies strongly. The almost complete loss of signals just below the surface at around 20 ns (about 1.2 m depth) from 20 to 150 m, from 330 to 360 m, and from 440 to 490 m are most likely related to changes in the road bed construction. The occurrence of strong diffraction hyperbola on this line (e.g., at 70, 160 and 430 m) is directly related to surficial objects like poles, bushes and trees as indicated by the derived wave velocity of 0.3 m/ns that corresponds to the wave velocity in air.

Upper slope (Fig. 1, line 2; GPR section: Fig. 5a)

Data

Towards the upper slope, reflection character changes abruptly. Continuous, mostly moderate-amplitude reflections

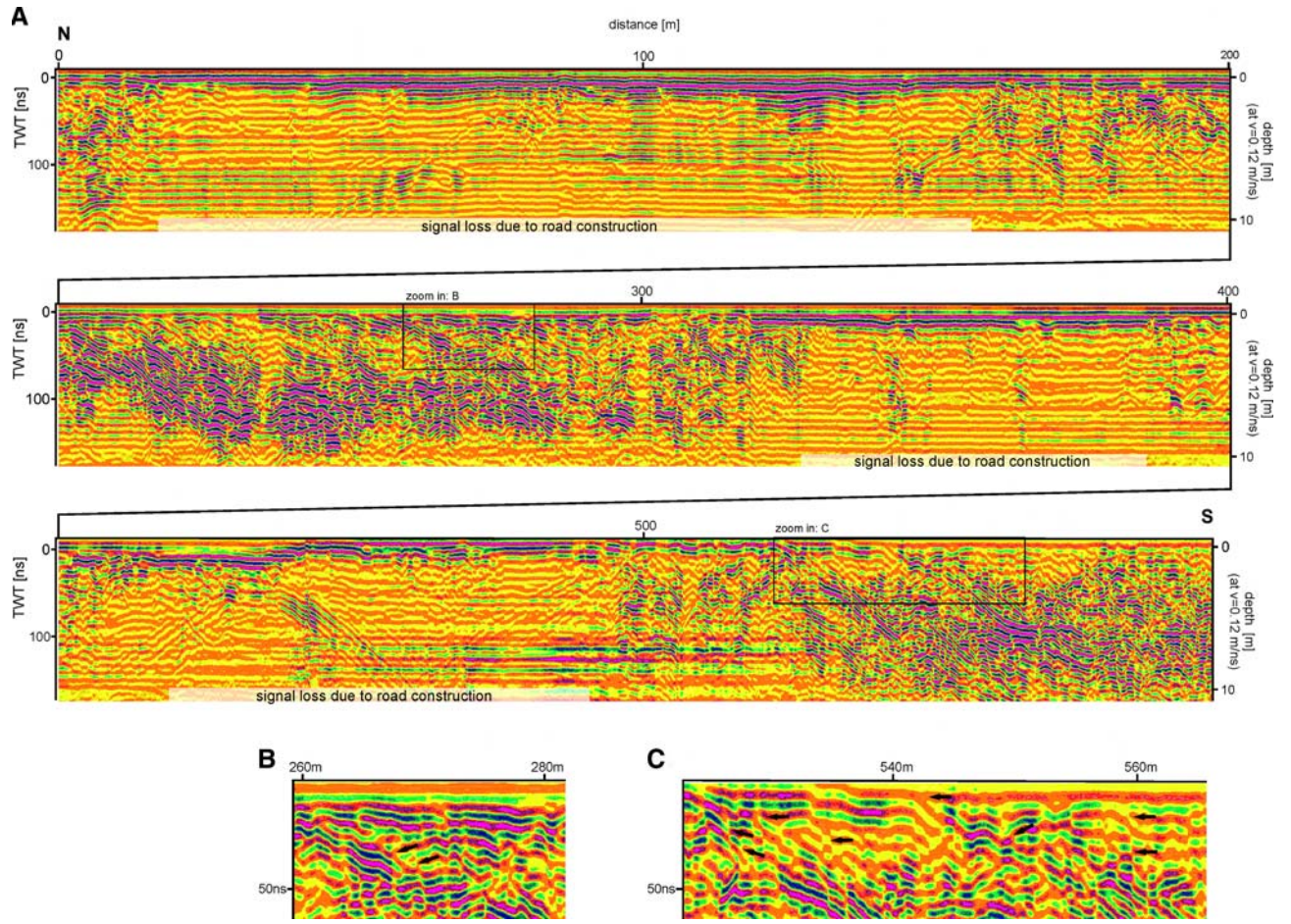

Fig. 4 GPR line 1. **a** 300 MHz GPR section of middle ramp to slope deposits over a length of 597 m. **b** Detail of section shown in **a** covers interval between 260 and 280 m and shows downlapping reflections (*black arrows*). **c** Detail of section shown in **a** covers interval between 552 and 563 m and shows onlapping and truncated reflections (*black arrows*). For a detailed discussion see text

are observed that dip basinward with angles of 18° (Fig. 5b). Here, penetration reaches its maximum with 500 ns (about 30 m depth). The angle of dip decreases towards the south to 14° in the upper part and below 200 ns the angle of dip decreases down to 5°–9° (Fig. 5b). Several bend bedding features are present (Fig. 5c) mostly in the northern part of the section. Starting at around 80 m the maximum depth of the radar signal is massively reduced. This loss of deeper information continues until the end of the section.

Interpretation

The GPR does not show each individual foreset unit as seen in the outcrop (Fig. 3c), but reflects groups of dipping beds. The moderate-amplitude steeply dipping reflections (Fig. 5b) are interpreted to correspond to the coarse-grained rhodolitic clinobeds as seen in outcrop (Fig. 3b) where they show high porosity, which is in accordance with the mostly moderate-amplitude character of the reflections and their homogenous appearance. The radar section confirms the progradational character of the rhodolite clinobeds that here are shown to uniformly prograde over a distance of almost 100 m, so that the information from cliff outcrops is extended by the radar data. A reason for the maximum TWT (penetration depth) observed here might be a homogeneous residual water content resulting from the high porosity that resulted in good coupling of the radar signal; at the same time porosity and low clay mineral content resulted in low attenuating of the signal.

The observed bent bedding features (Fig. 5c) have been subdivided into three categories: longshore dunes, slumping features and contorted bedding. The longshore dunes which were described by Pomar et al. (2002) are characterized by a concave-upward shape sitting on continuous dipping reflectors that are not disturbed by the on sitting structure. A misinterpretation of a diffraction hyperbola resulting from a point reflector is excluded, as this would show some disturbances at the hyperbola arms influencing the underlying reflectors.

Slumping features are characterized by a sudden steep dip against the slope, whereas the reflection directly basinward again shows the regular slope dip angle and direction. This results in a kind of flat lying s-shape structure. A tectonic interpretation is rejected because the feature could not be traced to greater a depth in the section. This is in accordance with the outcrop observations of Pomar et al. (2002).

The other contorted bedding features are dominant in the lower intervals of the northern part of the section indicating slope instability due to the high sediment supply.

The signal loss starting at around 90 m and a depth of around 200 ns is interpreted as outer ramp deposits. These deposits attenuate due to their finer grain size and slightly higher clay content the radar signal in a much stronger way. In addition diffraction hyperbola analysis indicates a wave velocity of 0.08 m/ns that is significantly lower than the average wave velocity of 0.12 m/ns and thus indicates a change in lithology.

The section clearly shows the internal architecture of the slope not visible in the outcrops. It demonstrates the subdivision in an aggradational package to the north and a progradational package to the south. Both packages are separated by a downlap surface (Fig. 5d). From the section the estimated length of the progradational unit is minimum 150 m which correlates with the outcrop observation.

Implications and conclusions

The study of the Menorcan carbonate ramp with large distance–deep penetration GPR sections demonstrates that GPR is a valuable tool for extrapolating information from outcrops and wells. The data gathered with the GPR provides information on the subsurface sedimentary structures, and allows refining the preexisting carbonate ramp depositional model of the Lower Tortonian of Menorca of Pomar et al. (2002, 2004). The GPR approach additionally allows characterizing heterogeneities larger than outcrop scale.

The radar sections show characteristic features for the different depositional environments and reveal details on the deposits on a nearly 100 m long, continuous horizontal section. These features are interpreted as analogous to those known from outcrop of the respective depositional environments. The value of the radar sections here is that they allow extrapolation of outcrop data into areas where these sediments are not directly accessible. Thus, the depositional model of the Tortonian ramp of Menorca (Pomar et al. 2002) was verified and refined.

New information from the GPR data includes the proof of the lateral extent of uniform progradation of the rhodolite clinobeds. The lateral continuity of this progradational feature has previously been deduced from cliff outcrops, but the proof of this uniform progradation is now possible with the GPR. The abrupt transition from the middle ramp to upper slope clinobeds is well visualized on the radar section. Here, the radar data provide a much clearer image than the outcrops. In this GPR study, the existence, geometry, and dimensions of 3D dunes are constrained.

Our study also demonstrates that preexisting knowledge is required for fully recognizing the value of the GPR data for interpretation and prediction. Our study successfully recorded the internal anatomy of a prograding carbonate ramp with GPR. It enables us to verify and refine the preexisting ramp model. True 3D surveys with high-

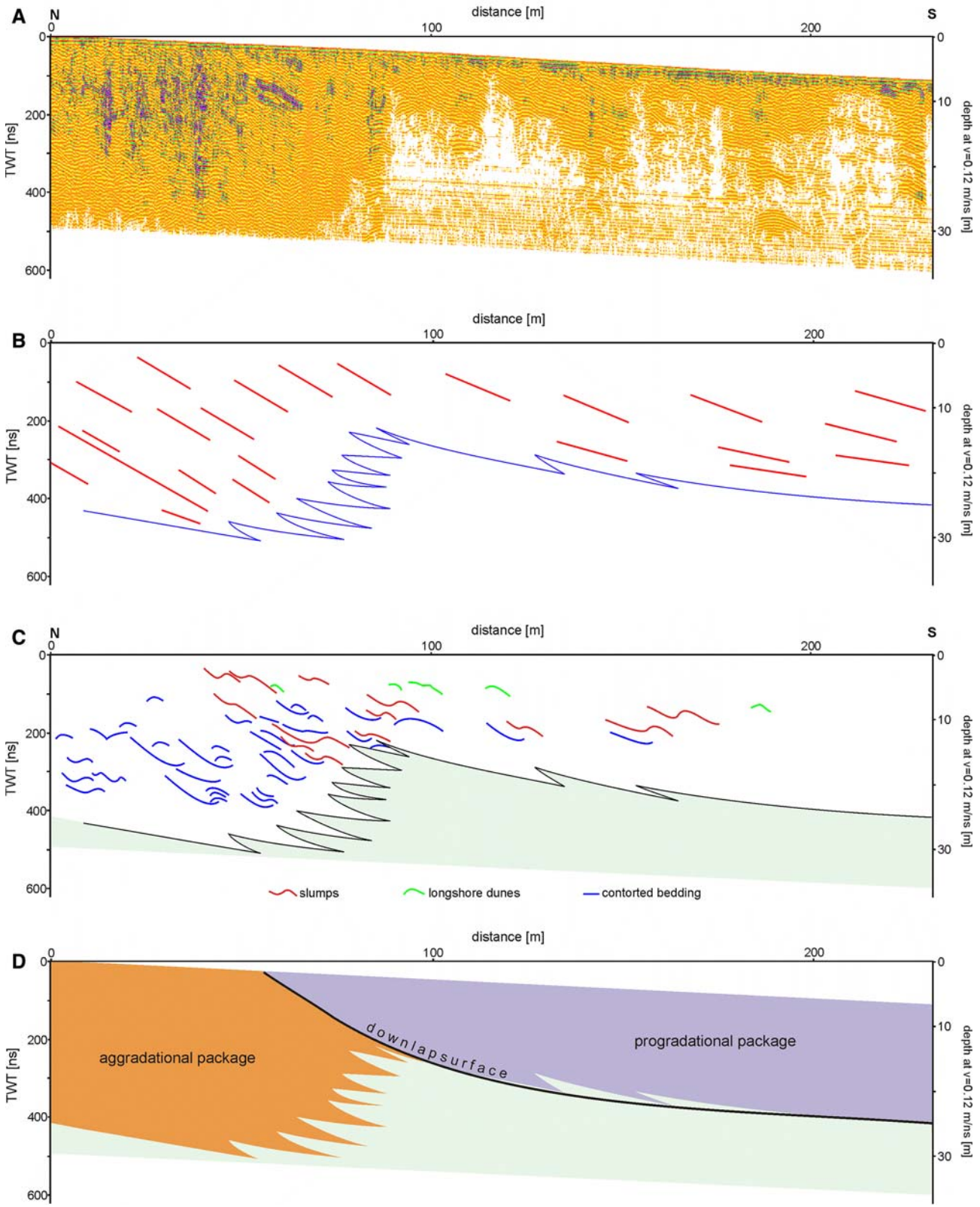

Fig. 5 GPR line 2. 300 MHz GPR section of ramp slope deposits. **a** GPR data. **b** Change of angle of dip from north to south. **c** Details of the GPR line showing bent bedding features. **d** Sequence stratigraphic subdivision of the measured section

resolution GPR grids would be the next step in studying the carbonate ramp in detail.

Acknowledgments Fynn Surlyk and an anonymous referee are thanked for their helpful comments. Antonio Obrador and Christian Schmidt are thanked for help in the field and Thomas Aigner for lending us his GPR equipment. This work was partly supported by the "Freunde der Universität Hannover" to MN, and DGI CGL2005-00537/BTE Spanish project to LP. Part of the work presented here is from MN's MSc thesis.

References

Anselmetti FS, Eberli GP (1993) Controls on sonic velocity in carbonates. Pure Appl Geophys 141:287–323. doi:10.1007/BF00998333

Ashley GM (1990) Classification of large-scale subaqueous bedforms: a new look at an old problem. J Sediment Petrol 60:160–172

Asprion U (1998) Ground-penetrating radar (GPR): analysis in aquifer-sedimentology: case studies with an emphasis on glacial systems of SW Germany. Tübinger Geologische Abh 43:1–105

Asprion U, Aigner T (1997) Aquifer architecture analysis using ground penetrating radar: Triassic and Quaternary examples (S-Germany). Environ Geol 31:66–75. doi:10.1007/s002540050165

Asprion U, Aigner T (2000) An initial attempt to map carbonate buildups using ground-penetrating radar: an example from the Upper Jurassic of SW-Germany. Facies 42:245–252. doi:10.1007/BF02562575

Barón A, Pomar L (1985) Area 2c Balearic depression. In: Steininger FF, Senes J, Kleemann K, Rog F (eds) Stratigraphic correlation tables, Neogene of the Mediterranean, Tethys and Parathetys 1: 17 and 2: 17, University of Vienna

Borgomano J, Masse J-P, Al Maskiry S (2002) The lower Aptian Shuaiba carbonate outcrops in Jebel Akhdar, northern Oman: Impact on static modeling for Shuaiba petroleum reservoirs. AAPG Bull 86:1513–1529

Brandano M, Vannucci G, Pomar L, Obrador A (2005) Rhodolith assemblages from the lower Tortonian carbonate ramp of Menorca (Spain): environmental and paleoclimatic implications. Palaeogeogr Palaeoclimatol Palaeoecol 226:307–323. doi:10.1016/j.palaeo.2005.04.034

Bristow C (1995) Facies analysis in a Lower Greensand using ground-penetrating radar. J Geol Soc London 152:591–598. doi:10.1144/gsjgs.152.4.0591

Buynevich IV, Fitzgerald DM (2003) High-resolution subsurface (GPR) imaging and sedimentology of coastal ponds, Maine, USA: implications for Holocene back-barrier evolution. J Sediment Res B73:559–571. doi:10.1306/121802730559

Conyers LB, Goodman D (1997) ground-penetrating radar: an introduction for archaeologists. Altamira Press, London, 232 p

Corbeanu RM, Soegard K, Szerbiak RB, Thurmond JB, McMechan GA, Wang D et al (2001) Detailed internal architecture of a fluvial channel sandstone determined from outcrop, cores, and 3-D ground-penetrating radar: example from the middle Cretaceous Ferron Sandstone, east-central Utah. AAPG Bull 85:1583–1608

Cunningham KJ (2004) Application of ground-penetrating radar, digital optical borehole images, and cores for characterization of porosity hydraulic conductivity and paleokarst in the Biscayne aquifer, southeastern Florida, USA. J Appl Geophys 55:61–76. doi:10.1016/j.jappgeo.2003.06.005

Dagallier G, Laitinen A, Malarte F, Campenhout I, Veeken P (2000) Ground penetrating radar application in a shallow marine Oxfordian limestone sequence located on the Eastern Flank of the Paris Basin, NE-France. Sediment Geol 130:149–165. doi:10.1016/S0037-0738(99)00105-0

Davis JL, Annan AP (1989) Ground-penetrating radar for high-resolution mapping of soil and rock stratigraphy. Geophys Prospect 37:531–551. doi:10.1111/j.1365-2478.1989.tb02221.x

Grandjean G, Gourry JC, Bitri A (2000) Evaluation of GPR techniques for civil-engineering applications: study on a test site. J Appl Geophys 45:141–156. doi:10.1016/S0926-9851(00)00021-5

Grasmück MP (1992) Beispiele zur Anwendung von Georadar in der Quartärgeologie. Eclogae geologicae Helveticae 85:471–490

Grasmueck M, Weger R (2002) 3D GPR reveals complex internal structure of Pleistocene oolitic sandbar. Lead Edge Explor 21:634–639. doi:10.1190/1.1497315

Haq BU, Hardenbol J, Vail PV (1988) Mesozoic and Cenozoic chronostratigraphy and cycles of sea-level change. In: Wilgus CK, Hastings BS, Kendall CGStC, Posamentier HW, Ross CA, Van Wagoner JC (eds), Sea-level changes: an integrated approach, vol 42. SEPM Spec Pub, pp 71–108

Huggenberger P, Meier E, Pugin A (1994) Ground-probing radar as a tool for heterogeneity estimation in gravel deposits: advances in data-processing and facies analysis. J Appl Geophys 31:131–184. doi:10.1016/0926-9851(94)90056-6

Kenter JAM, Fouke BW, Reinders M (1997) Effects of differential cementation on the sonic velocities of upper Cretaceous skeletal grainstones (southeastern Netherlands). J Geophys Res 67:178–185

Liner C, Liner J (1995) Ground-penetrating radar: a nearface experience from Washington County, Arkansas. Lead Edge (Tulsa Okla) (Jan):17–21. doi:10.1190/1.1437057

Mateu-Vicens G, Hallock P, Brandano M (2008) A depositional model and paleoecological reconstruction of the Lower Tortonian distally steepened ramp of Menorca (Balearic Islands, Spain). Palaios 23:465–481. doi:10.2110/palo.2007.p07-061r

Mazzullo SJ (1998) Stratigraphic architecture of Lower Permian, cyclic carbonate reservoirs (Chase Group) in the mid-continent USA, based on outcrop studies. AAPG Bull 82:464–483

McMechan GA, Gaynor G, Szerbiak RB (1997) Use of ground-penetrating radar for 3-D sedimentological characterization of clastic reservoir analogs. Geophysics 62:786–796. doi:10.1190/1.1444188

Milsom J (1996) Field geophysics. Wiley, New York, 187 p

Neal A (2004) Ground-penetrating radar and its use in sedimentology: principles, problems and progress. Earth Sci Rev 66:261–330. doi:10.1016/j.earscirev.2004.01.004

Nielsen L, Boldreel LO, Surlyk F (2004) Ground-penetrating radar imaging of carbonate mound structures and implications for interpretation of marine seismic data. AAPG Bull 88:1069–1082. doi:10.1306/02230403070

Obrador A (1972–1973) Estudio estratigráfico y sedimentológico de los materiales miocénicos de la Isla de Menorca. Revista de Menorca 64: 37–197 and 65: 35–97 and 125–189

Obrador A, Pomar L, Rodriguez A, Jurado M (1983) Unidades deposicionales del Neógeno menorquin. Acta Geol Hisp 18:87–97

Obrador A, Pomar L, Taberner C (1992) Late Miocene breccia of Menorca (Balearic Islands): a basis for the interpretation of a Neogene ramp deposit. Sediment Geol 79:203–223. doi:10.1016/0037-0738(92)90012-G

Pomar L (1991) Reef geometries, erosion surfaces and high-frequency sea-level changes, upper Miocene Reef Complex, Mallorca, Spain. Sedimentology 38:243–269. doi:10.1111/j.1365-3091.1991.tb01259.x

Pomar L (2001) Ecological control of sedimentary accommodation: evolution from carbonate ramp to rimmed shelf, Upper Miocene, Balearic Islands. Palaeogeogr Palaeoclimatol Palaeoecol 175:249–272. doi:10.1016/S0031-0182(01)00375-3

Pomar L, Marzo M, Barón A (1983) El Terciario de Mallorca. In: Pomar L, Obrador A, Fornós J, Rodriguez-Perea A (eds) El Terciario de las Baleares. Libro Guia de las Excursiones del X Con. Nac. Sedimentología. Maó: 21–44

Pomar L, Ward WC, Green DG (1996) Upper Miocene Reef Complex of the Llucmajor area, Mallorca, Spain. In: Franseen E, Esteban M, Ward WC, Rouchy JM (eds) Models for carbonate stratigraphy from Miocene Reef Complexes of the Mediterranean regions. SEPM concepts in sedimentology and paleontology series 5: 191–225

Pomar L, Obrador A, Westphal H (2002) Sub-wavebase cross-bedded grainstones on a distally steepened carbonate ramp, Upper Miocene, Menorca, Spain. Sedimentology 49:139–169. doi: 10.1046/j.1365-3091.2002.00436.x

Pomar L, Brandano M, Westphal H (2004) Environmental factors influencing skeletal grain sediment associations: a critical review of Miocene examples from the western Mediterranean 51: 627–651

Pratt BR, Miall AD (1993) Anatomy of a bioclastic grainstone megashoal (Middle Silurian, southern Ontario) revealed by ground-penetrating radar. Geology 21:223–226. doi:10.1130/0091-7613(1993)021<0223:AOABGM>2.3.CO;2

Read JF (1985) Carbonate platform facies models. AAPG Bull 69:1–21

Reynolds JM (1997) An introduction to applied and environmental geophysics. Wiley, Chichester, 796 p

Stoudt EL, Harris PM (1994) Hydrocarbon reservoir characterization; geologic framework and flow unit modeling. SEPM short course notes 34: 357

Stephens M (1994) Architectural element analysis within the Kayenta Formation (Lower Jurassic): using ground-probing radar and sedimentological profiling, Southwestern Colorado. Sediment Geol 90:179–211. doi:10.1016/0037-0738(94)90038-8

Van Dam RL, Schlager W (2000) Identifying causes of ground-penetrating radar reflections using time-domain reflectometry and sedimentological analyses. Sedimentology 47:435–449. doi: 10.1046/j.1365-3091.2000.00304.x